Published OnlineFirst May 22, 2017; DOI: 10.1158/1078-0432.CCR-16-2253

Cancer Therapy: Preclinical

Clinical Cancer Research

Multifunctional Effects of a Small-Molecule STAT3 Inhibitor on NASH and Hepatocellular Carcinoma in Mice

Kwang Hwa Jung[1], Wonbeak Yoo[1], Heather L. Stevenson[2], Dipti Deshpande[1], Hong Shen[1], Mihai Gagea[3], Suk-Young Yoo[4], Jing Wang[4], T. Kris Eckols[5], Uddalak Bharadwaj[5], David J. Tweardy[1,5], and Laura Beretta[1]

Abstract

Purpose: The incidence of hepatocellular carcinoma is increasing in the United States, and liver cancer is the second leading cause of cancer-related mortality worldwide. Nonalcoholic steatohepatitis (NASH) is becoming an important risk for hepatocellular carcinoma, and most patients with hepatocellular carcinoma have underlying liver cirrhosis and compromised liver function, which limit treatment options. Thus, novel therapeutic strategies to prevent or treat hepatocellular carcinoma in the context of NASH and cirrhosis are urgently needed.

Experimental Design: Constitutive activation of STAT3 is frequently detected in hepatocellular carcinoma tumors. STAT3 signaling plays a pivotal role in hepatocellular carcinoma survival, growth, angiogenesis, and metastasis. We identified C188-9, a novel small-molecule STAT3 inhibitor using computer-aided rational drug design. In this study, we evaluated the therapeutic potential of C188-9 for hepatocellular carcinoma treatment and prevention.

Results: C188-9 showed antitumor activity *in vitro* in three hepatocellular carcinoma cell lines. In mice with hepatocyte-specific deletion of *Pten* (Hep*Pten*$^{-}$ mice), C188-9 treatment blocked hepatocellular carcinoma tumor growth, reduced tumor development, and reduced liver steatosis, inflammation, and bile ductular reactions, resulting in improvement of the pathological lesions of NASH. Remarkably, C188-9 also greatly reduced liver injury in these mice as measured by serum aspartate aminotransferase and alanine transaminase levels. Analysis of gene expression showed that C188-9 treatment of Hep*Pten*$^{-}$ mice resulted in inhibition of signaling pathways downstream of STAT3, STAT1, TREM-1, and Toll-like receptors. In contrast, C188-9 treatment increased liver specification and differentiation gene pathways.

Conclusions: Our results suggest that C188-9 should be evaluated further for the treatment and/or prevention of hepatocellular carcinoma. *Clin Cancer Res; 23(18); 5537–46. ©2017 AACR.*

Introduction

Hepatocellular carcinoma is the second most common cause of cancer-related deaths worldwide (1). Although the highest rates of liver cancer are found in certain areas of Asia and Africa, liver cancer incidence and mortality rates are increasing strikingly in western countries, including the United States (2, 3). Liver cirrhosis due to hepatitis B virus, hepatitis C virus, high alcohol consumption or nonalcoholic steatohepatitis (NASH) are the main risk factors associated with hepatocellular carcinoma; most patients with hepatocellular carcinoma have compromised liver function, which limits treatment options. Hepatocellular carcinoma is a complex and highly heterogeneous disease with a large spectrum of genomic alterations and aberrant activation of cell signaling pathways (4–6). Currently, effective treatment options for hepatocellular carcinoma are limited. Surgical resection or transplantation represent the only potentially curative therapies for hepatocellular carcinoma, but most patients are diagnosed at an advanced stage and are not candidates for these approaches. Thus, there is a pressing need for the development of novel approaches to treat and prevent hepatocellular carcinoma (7, 8).

The pivotal role of STAT3 in cancer development and progression in many human cancers has led to intense efforts to identify small molecules and other strategies for targeting STAT3 (9–11). STAT3 is a transcription factor that regulates cell proliferation and survival as well as immune responses associated with cancer development and progression including hepatocellular carcinoma. Nearly 60% of human hepatocellular carcinoma exhibit activated nuclear STAT3 and STAT3 activation is associated with a poor prognosis (12, 13). The critical role of STAT3 as a regulator of liver cancer development and progression was demonstrated in mice (13, 14). STAT3 has also been linked to liver inflammation, injury, and regeneration and to the activation of hepatic stellate cells (15–17).

[1]Department of Molecular and Cellular Oncology, The University of Texas MD Anderson Cancer Center, Houston, Texas. [2]Department of Pathology, University of Texas Medical Branch, Galveston, Texas. [3]Department of Veterinary Medicine & Surgery, University of Texas MD Anderson Cancer Center, Houston, Texas. [4]Department of Bioinformatics and Computational Biology, The University of Texas MD Anderson Cancer Center, Houston, Texas. [5]Department of Infectious Diseases, Infection Control, and Employee Health, The University of Texas MD Anderson Cancer Center, Houston, Texas.

Note: Supplementary data for this article are available at Clinical Cancer Research Online (http://clincancerres.aacrjournals.org/).

K.H. Jung and W. Yoo contributed equally to this article.

Corresponding Author: Laura Beretta, The University of Texas MD Anderson Cancer Center, 1515 Holcombe Boulevard, Houston, TX 77030. Phone: 713-792-9100; Fax: 713-794-4023; E-mail: lberetta@mdanderson.org

doi: 10.1158/1078-0432.CCR-16-2253

Published OnlineFirst May 22, 2017; DOI: 10.1158/1078-0432.CCR-16-2253

Translational Relevance

The incidence of hepatocellular carcinoma is increasing in the United States and is the second leading cause of cancer-related mortality worldwide. Nonalcoholic steatohepatitis (NASH) is becoming an important risk for hepatocellular carcinoma, and most patients with hepatocellular carcinoma have underlying liver cirrhosis and compromised liver function, which limit treatment options. Thus, novel therapeutic strategies to prevent or treat hepatocellular carcinoma in the context of NASH and cirrhosis are urgently needed. This study identified the novel small-molecule C188-9 as a highly promising therapeutic drug for treatment and prevention of hepatocellular carcinoma. C188-9 showed not only preventive and antitumor activity but also significant reduced pathologic lesions of NASH and hepatocellular injury, with an overall improvement of liver functions. This dual effect of C188-9 may be highly beneficial to patients with hepatocellular carcinoma with NASH or liver cirrhosis. A phase 1 trial will be initiated later this year to examine the potential of C188-9 treatment in patients with hepatocellular carcinoma.

In a drug development program involving virtual ligand screening, two-dimensional (2-D) similarity screening, 3-D pharmacophore analysis, and SAR-based medicinal chemistry, we identified C188-9 as a potent small-molecule that targets the Src-homology (SH) 2 domain of STAT3 (18–21). C188-9 inhibited growth and survival of several cancer cell lines *in vitro*, including breast cancer (18), acute myeloid leukemia (19), head and neck squamous cell carcinoma (20) and non–small cell lung cancer (21). To test the effects of C188-9 on hepatocellular carcinoma and underlying liver disease, we herein used mice with hepatocyte-specific deletion of *Pten* (Hep*Pten*$^{-}$ mice). These mice present with hepatomegaly and develop liver disease marked by steatosis, inflammation, and fibrosis characteristic of NASH, which progresses to development of hepatocellular carcinoma (22–25). This is a highly relevant model for preclinical studies of hepatocellular carcinoma in the context of steatosis, fibrosis or NASH (26, 27).

Materials and Methods

Cell culture and MTT viability assays

Human hepatoma cell lines Huh7 (ATCC), and PLC/PRF/5 and hepatoblastoma cell line HepG2 (ATCC) were grown in DMEM (Invitrogen) supplemented with 10% FBS, 100 units/mL penicillin, and 100 μg/mL streptomycin. The hepatic epithelial cells THLE3 (ATCC) were grown and maintained in BEGM+ (Lonza/Clonetics Corp.) but cultured in complete DMEM when assays were performed. For cell viability assays, cells were treated in 96-well plates in medium ± C188-9 (StemMed, Ltd.) for 48 hours and subjected to MTT assays. Briefly, cells were incubated with 0.5 mg/mL of the MTT solution (Sigma) for 2 hours and cell viability was measured by optical density (OD) at 590 nm (SpectraMax Plus 384 Microplate Reader, Molecular Devices). Experiments were performed in triplicate and used for IC_{50} calculation using GraphPad software.

Mice treatment and MR imaging

The study was approved by our Institutional Animal Care and Use Committee (IACUC). C57BL/6 mice carrying *Pten* conditional knockout alleles were crossed with an Albumin (Alb)-Cre-transgenic mouse. For this model, control animals are *Pten*$^{loxP/loxP}$; Alb-Cre^{-}, whereas the experimental mice are *Pten*$^{loxP/loxP}$; Alb-Cre^{+}. For *in vivo* treatment, C188-9 was dissolved in DMSO, and hepatic *Pten* null mice (Hep*Pten*$^{-}$mice; 11 month-old) received C188-9 (100 mg/kg) or vehicle (DMSO) by intraperitoneal injection daily for 4 weeks. Each treatment group included 9 to 12 mice. In a separate prevention study, Hep*Pten*$^{-}$ mice (8 months old) received C188-9 (50 mg/kg) or DMSO by intraperitoneal injection daily for 4 weeks. MRI was performed at the beginning of treatment and repeated after 2 and 4 weeks, on a four-channel, 7T dedicated small animal scanner (Bruker Biospin MRI). For tumor detection, a rapid acquisition with relaxation enhancement (RARE) sequence was used in the coronal and axial planes with a 0.25-mm slice thickness and with the number of slices sufficient to cover the entire liver. For respiration monitoring, a pressure-sensitive pad was placed on the animal bed directly underneath the animal. The compression and decompression of the pad were measured, and the generated signal was finally fed to the MRI scanner.

Liver histopathology, IHC, and liver function assays

ACUC-endorsed euthanasia by CO_2 was performed followed by necropsy at which time, liver and tumor tissues were collected and snap-frozen in liquid nitrogen or fixed in 10% neutral buffered formalin and paraffin embedded (FFPE). The snap-frozen tissues were pulverized for RNA or protein extraction. FFPE tissues were sectioned in 4-μm-thick histologic sections that were stained with hematoxylin and eosin (H&E) or Masson's trichrome staining. Histopathologic analysis was performed blindly by a liver pathologist. A NAFLD Activity Score (NAS) was described for scoring liver biopsies in patients with steatosis/steatohepatitis (28). In most cases of human NASH, the majority of the steatosis is of the macrovesicular type. Although focal areas of microvesicular steatosis can be seen, this is not a common component of the steatosis in human disease. In contrast, some mouse models of NASH, including the Hep*Pten*$^{-}$ model, have mixed macrovesicular and microvesicular steatosis. We therefore used a modified NAFLD activity score (mNAS) to include both macrovesicular and microvesicular steatosis grades, calculated as an unweighted sum of the grading scores of macrosteatosis (0–3), microsteatosis (0–3), grade of lobular inflammation (0–3), and presence of ballooning (0–2). Bile ductular reaction was assessed on a 1 to 4 scale. Blood samples were also taken at necropsy and processed for serum collection. Serum aspartate aminotransferase (AST) and alanine transaminase (ALT) activities were determined using ACE AXCEL clinical chemistry system (Diagnostic Technologies) according to the manufacturer's instructions. Standard controls were run before each determination, and the values obtained for the biochemical parameter were within the expected ranges. IHC staining for Ki67 was performed using vehicle- and C188-9-treated tumor slides. Slides were scanned and analyzed using Aperio ImageScope software. The proliferation index was determined by calculating the average percentage of Ki67 tumor positive cells.

RNA sequencing and differentially expressed gene analysis

Total RNA was isolated from liver and tumors of the study mice. Following second-strand cDNA synthesis, end repair, adaptor ligation, and PCR amplification, the enriched cDNA

Published OnlineFirst May 22, 2017; DOI: 10.1158/1078-0432.CCR-16-2253

libraries were sequenced using Illumina HiSeq 3000. Libraries were run using 50-base-pair single-end reads on Illumina HiSeq 3000 System. Sequence files were generated in FASTQ format, and reads were mapped to mouse genome mm10 and then aligned by TopHat2 (29). Gene expression levels were quantified using Cufflinks (version 1.0.3) in the FPKM unit (fragments per kilobase of exon per million fragments mapped) together with confidence intervals. Cufflinks ran in the default parameters except that the annotated gene set was supplied using the -G option. Subsequently, the empirical analysis of digital gene expression data in R (edgeR) tool was utilized to detect the differentially expressed genes (DEG) after filtering out genes with counts per million (CPM) under 10 in all samples. CPM values were scaled by the total number of fragments. The multiple comparison *P* values were adjusted by using Benjamini–Hochberg method, providing a *P* value cutoff for significance controlled by the FDR. DEGs were selected using the following criteria: FDR < 0.05 and fold change > 1.5. The heat map of DEGs was generated using Pearson correlation and Ward distance in *R* and CPM values. DEGs were further analyzed using the ingenuity pathway analysis (IPA) software (Ingenuity Systems; http://www.ingenuity.com). IPA identifies putative networks, biological functions, and canonical pathways overrepresented among the DEGs.

Luminex assays

Cell and tissue lysates were plated in a 96-well filter plate preloaded with beads (Millipore) coupled to antibody against the indicated analytes and incubated overnight at 4°C. Bead-bound analytes were measured using biotinylated detection antibody specific for a different epitope and streptavidin-phycoerythrin (streptavidin-PE; refs. 30, 31). Data were collected and analyzed using the Bio-Plex suspension array system (Luminex 100 system, Bio-Rad Laboratories). GAPDH-normalized pY-STAT1 and pY-STAT3 values from the treated samples were compared to the untreated samples. Serum cytokine levels were measured using Luminex MAP assays (MILLIPLEX MAP Mouse Cytokine/Chemokine, MCYTOMAG-70K, Millipore) and 25 μL of serum samples. The assay was performed on a Luminex 200 instrument (Luminex Corp.) using Luminex xPONENT 3.1 software. Using the standard curves for the given cytokine or chemokine, we obtained absolute concentrations for the various experimental conditions for all analytes measured.

Quantitative PCR

To quantify selected mRNA levels, equal amounts of total RNA samples were submitted to reverse transcription and real-time PCR using specific primers listed in Supplementary Table S1. PCR amplifications of the respective genes were performed using iTaq SYBR Green Supermix (Bio-Rad) in CFX Connect Real-Time System (Bio-Rad). The Bio-Rad CFX Manager software (version 2.1) was used for the calculation of threshold cycles (Ct) values and melting curve analysis of amplified DNA. Relative expression of the tested miRNAs and genes was calculated by $2^{-\Delta\Delta C_t}$ method.

Statistical analysis

Statistical difference between each group was assessed by the nonparametric Mann–Whitney test using Graphpad 6.0 software. The high-throughput sequencing data were analyzed using the two-sample *t* test. A value of $P < 0.05$ was considered significant.

Results

C188-9 reduced hepatoma cell viability

To evaluate the potential of C188-9 as a therapeutic strategy for hepatocellular carcinoma, we first examined the effect of C188-9, a potent, nontoxic, inhibitor of STAT3, on the viability of the hepatoma cell lines Huh7 and PLC/PRF/5 and the hepatoblast-derived cells HepG2. All three cell lines had increased activated STAT3 (>2-fold), when compared to the normal hepatic epithelial cells THLE3 (Fig. 1A). We then treated them with C188-9 at serial concentrations ranging from 0.19 to 100 μmol/L, for 48 hours under anchorage-dependent condition. C188-9 reduced cell viability of all three cell lines with IC_{50} values of 11.27, 10.19, and 11.83 μmol/L for Huh7, PLC/PRF/5, and HepG2, respectively (Fig. 1B). Finally, we confirmed the inhibition of pSTAT3 levels in these cells upon C188-9 treatment. At 10 μmol/L, pSTAT3 levels were reduced by 25.4%, 25.1%, and 13.2% and at 30 μmol/L, pSTAT3 levels were reduced by 43.9%, 66.5%, and 81.1%, in Huh7, PLC/PRF/5, and HepaG2 cells, respectively (Fig. 1C).

C188-9 treatment resulted in tumor growth arrest in mice with hepatic deletion of *Pten*

We then evaluated the effect of targeting STAT3 *in vivo*, using the Hep*Pten*$^{-}$ mouse model. We treated 11-month-old Hep*Pten*$^{-}$ male mice for 4 weeks, with daily intraperitoneal injections of C188-9 or vehicle. All treated mice had developed tumors prior to treatment as confirmed by MRI. MRI imaging showed continuous tumor growth increase in vehicle-treated mice, but arrest of tumor growth in C188-9-treated mice (Fig. 2A). Indeed, although the average tumor growth rate in the vehicle group was 2.06-fold over 14 days, the average tumor growth rate was 1.16-fold in the C188-9 treated group ($P < 0.001$; Fig. 2B). The tumor growth arrest induced by C188-9 treatment was further confirmed by comparing the average tumor volume determined by MRI in both groups prior to treatment (119.02 and 92.64 mm^3 for vehicle- and C188-9-treated mice, respectively; P = ns) and at the end of treatment (249.02 and 106.48 mm^3 for vehicle- and C188-9-treated mice, respectively; $P = 0.04$; Fig. 2C). Necropsy results showed that although 70% of the tumors collected at time of necropsy from the vehicle group were >100 mm^3, only 24.85% of the tumors in C188-9 treated mice were >100 mm^3 ($P = 0.02$; Fig. 2D). Necropsy results also showed a significant reduction of liver to body weight ratio in C188-9-treated group compared to vehicle-treated mice ($P = 0.02$), further supporting the reduction of tumor growth upon C188-9 treatment (Fig. 2E). Finally, blinded analysis of all tumors by a pathologist showed that C188-9 treatment resulted in decreased percentage of carcinomas upon C188-9 treatment (from 92.87% to 86.67%) and concomitant increased percentage of adenomas (from 7.13% to 13.33%), indicating that tumor malignancy progression was inhibited upon C188-9 treatment (Fig. 2F).

C188-9 treatment improves NASH and liver function

Because Hep*Pten*$^{-}$ mice develop NASH prior to hepatocellular carcinoma, we also evaluated the effect of C188-9 treatment on this underlying liver pathology. The liver parenchyma in the vehicle-treated mice showed diffuse mixed macro- and micro-steatosis extending from zones 1 to 3 (Fig. 3A, a and b). In contrast, the C188-9-treated mice showed minimal steatosis, with only a few small foci of steatosis observed in the centrilobular area (Fig. 3A, arrows in c). As shown in Fig. 3B, steatosis scoring further

Published OnlineFirst May 22, 2017; DOI: 10.1158/1078-0432.CCR-16-2253

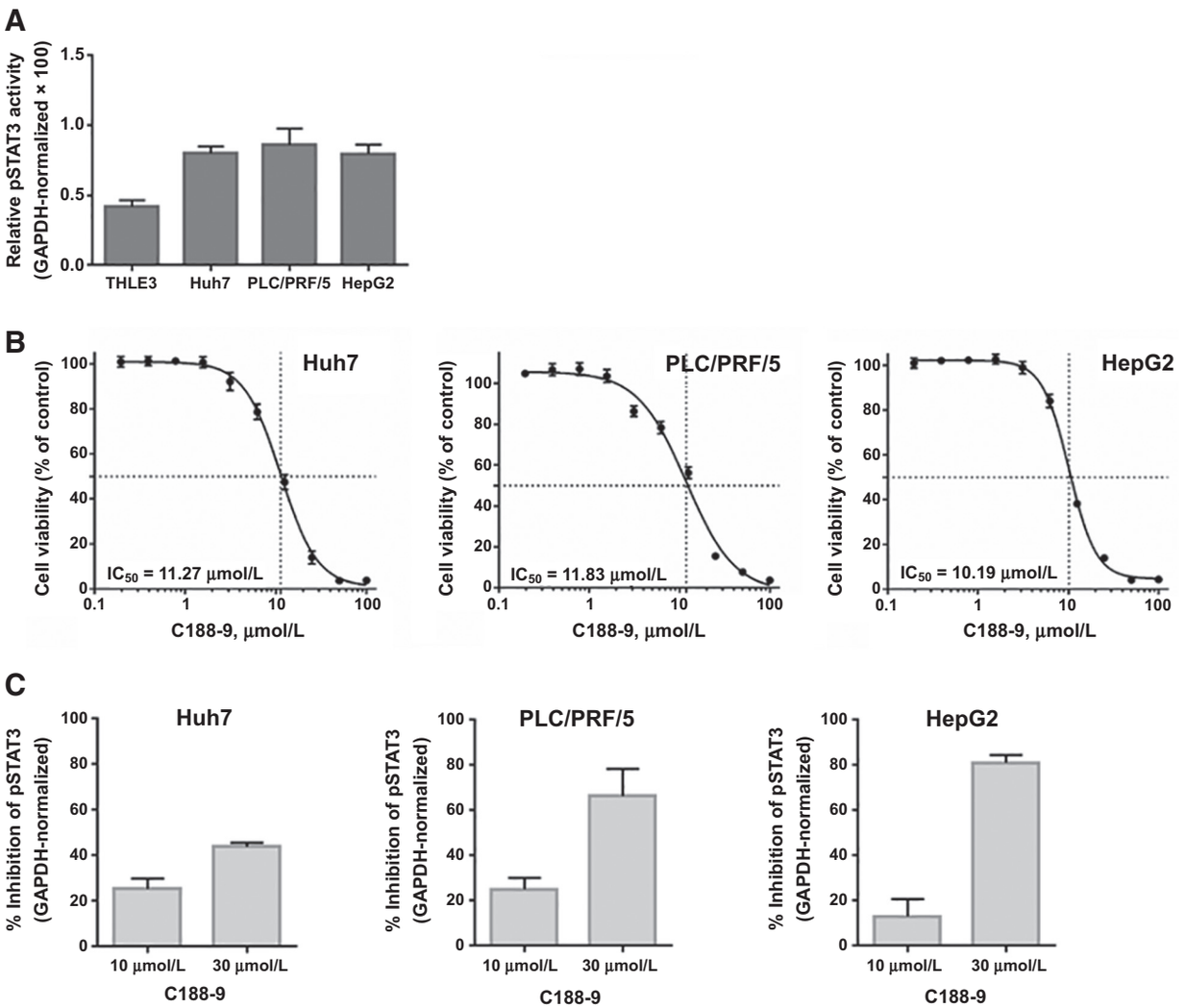

Figure 1.

C188-9 treatment reduced viability of hepatoma cells. **A,** Lysates prepared from asynchronous cultures of Huh7, PLC/PRF/5, HepG2 and THLE3 cells were examined for levels of pSTAT3 and GAPDH by luminex assay. GAPDH-normalized pSTAT3 levels of replicate experiments (×100) are shown in the Y-axis. **B,** Huh7, PLC/PRF/5, and HepG2 cell lines were treated with C188-9 at the concentrations indicated for 48 h under anchorage-dependent conditions. Cell viability was calculated as a percentage of the DMSO-treated control wells. The IC_{50} values were derived after plotting viability values on a logarithmic curve. **C,** Lysates prepared from Huh7, PLC/PRF/5 and HepG2 cells untreated or treated with 10 and 30 µmol/L of C188-9 were subjected to luminex-based detection of pSTAT3 and GAPDH levels. The GAPDH-normalized pSTAT3 levels of each treatment were expressed as a percent of untreated cells. Data shown are representative results of triplicate experiments for each cell line.

confirmed that C188-9 treatment resulted in a decrease in hepatic steatosis for both macrovesicular and microvesicular steatosis (2.7 ± 0.2 vs. 0.8 ± 0.2 and 2.7 ± 0.2 vs. 0.3 ± 0.2, respectively, $P < 0.001$ for both). In line with the effect of C188-9 on reducing the steatosis, ballooning of hepatocytes and inflammation were also significantly decreased in mice treated with C188-9 compared to vehicle-treated mice (1.8 ± 0.2 vs. 0.4 ± 0.2; $P = 0.002$ and 2 vs. 1 ± 0.3; $P = 0.016$). Using an mNAS to include both macrovesicular and microvesicular steatosis grades, we observed an overall inhibition of NASH and reversion to a phenotype with milder pathology upon C188-9 treatment (9.2 ± 0.3 vs. 2.4 ± 0.7; $P < 0.001$; Fig. 3B). The vehicle-treated mice also showed frequent areas of prominent bile ductular reaction with peribiliary neutrophilic inflammation (Fig. 3A, a and b). In contrast, most of the C188-9-treated mice appeared similar to untreated control mice, with the exception of rare focal bile ductular reactions, which had less associated inflammation and were significantly smaller in size when compared to those observed in the vehicle group (Fig. 3A, c and d). The bile ductular reaction scores were significantly reduced upon C188-9 treatment (2 vs. 0.6 ± 0.8; $P = 0.004$; Fig. 3C). In addition, C188-9 treatment significantly reduced fibrosis in these areas, measured by Masson's trichrome staining, from 8.77% to 3.07% ($P < 0.001$; Fig. A, panels a–d and 3D). Most remarkably and in agreement with NASH improvement, serum biochemical analysis showed a significant reduction of hepatocellular injury upon C188-9 treatment as ALT and AST

Published OnlineFirst May 22, 2017; DOI: 10.1158/1078-0432.CCR-16-2253

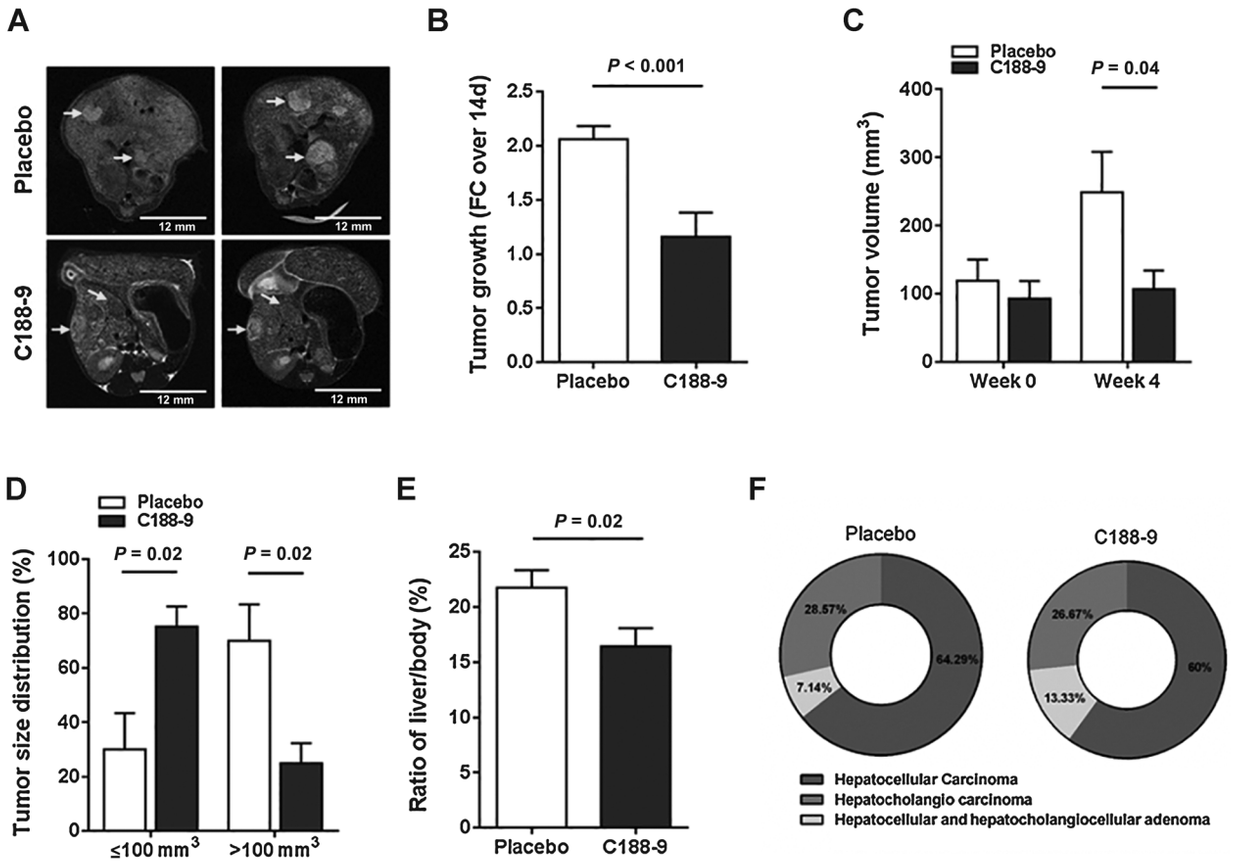

Figure 2.

Effect of C188-9 treatment on tumor growth and tumor phenotype. **A,** Liver of mice from vehicle- and C188-9-treated groups were imaged with MRI to measure tumor growth during treatment. Representative tumors detected by MRI before treatment and at the end of treatment, are indicated by yellow arrows. **B,** Tumor growth expressed as fold change over 2 weeks of treatment, in vehicle-treated and C188-9-treated groups as determined by MRI. **C,** Tumor volume before and after treatment as determined by MRI. **D,** Tumor size distribution in each treatment group. The tumors are separated into $\leq$100 mm^3 or >100 mm^3. Average percentages of tumors are represented on the Y-axis and tumor size categories on the X-axis. **E,** Liver-to-body weight ratio at the end of treatment. For panels **B** to **E**, data are presented as means $\pm$ SEM (Mann–Whitney test). **F,** Pie charts representing the overall tumor histology distribution within the two treatment groups.

levels decreased upon C188-9 treatment, from 434 to 165.43 IU/L ($P = 0.003$) and from 350 to 182.57 IU/L ($P = 0.004$), respectively (Fig. 3E), reaching near to normal values.

C188-9 treatment reduces tumor development *in vivo*

Because of the effects of C188-9 on NASH severity, we evaluated the effect of C188-9 on tumor development in the Hep*Pten*$^-$ mice. Mice without tumors as determined by MRI, were treated with C188-9 or vehicle and tumor development was monitored over a 4-week period by MRI. At the end of treatment, the average tumor size (6.24 ± 3.02 mm^3 vs. 25.25 ± 10.6 mm^3; $P = 0.05$) and average tumor burden (9.36 ± 5.67 mm^3 vs. 38.18 ± 17.76 mm^3) were lower in C188.9 treated mice compared to the vehicle group (Fig. 4), demonstrating that treatment of C188-9 reduces tumor development in Hep*Pten*$^-$ mice.

Gene expression changes upon C188-9 treatment in tumors and adjacent liver in Hep*Pten*$^-$ mice

To identify the mechanism of C188-9 effect *in vivo*, we measured mRNA expression using RNA-sequencing in both liver and tumors from C188-9-treated group and vehicle group. Using P value <0.05 and fold change >1.5, we identified 606 upregulated and 870 downregulated genes in liver and 478 upregulated and 172 downregulated genes in tumors, upon C188-9 treatment. Among these genes, 144 genes were commonly upregulated and 96 genes were commonly downregulated in both liver and tumor (Fig. 5A). Hierarchical clustering based on these DEGs distinguished four main clusters corresponding to vehicle liver, vehicle tumor, C188-9 tumor and C188-9 liver, with the widest separation being between vehicle liver and C188-9 liver. The clustering analysis demonstrated that all mice responded similarly to C188-9 treatment and that the effects on gene expression were largely specific to the liver or the tumor, with the largest effect being observed in liver (Fig. 5B).

We performed IPA for all DEGs significantly downregulated or upregulated or in liver, in tumor, or in both. The top biological functions and canonical pathways that were downregulated by C188-9 were TREM1 signaling, role of pattern recognition receptors in recognition of bacteria and viruses in liver; cellular growth and cell death and survival in tumor; mitotic role of polo-like

Published OnlineFirst May 22, 2017; DOI: 10.1158/1078-0432.CCR-16-2253

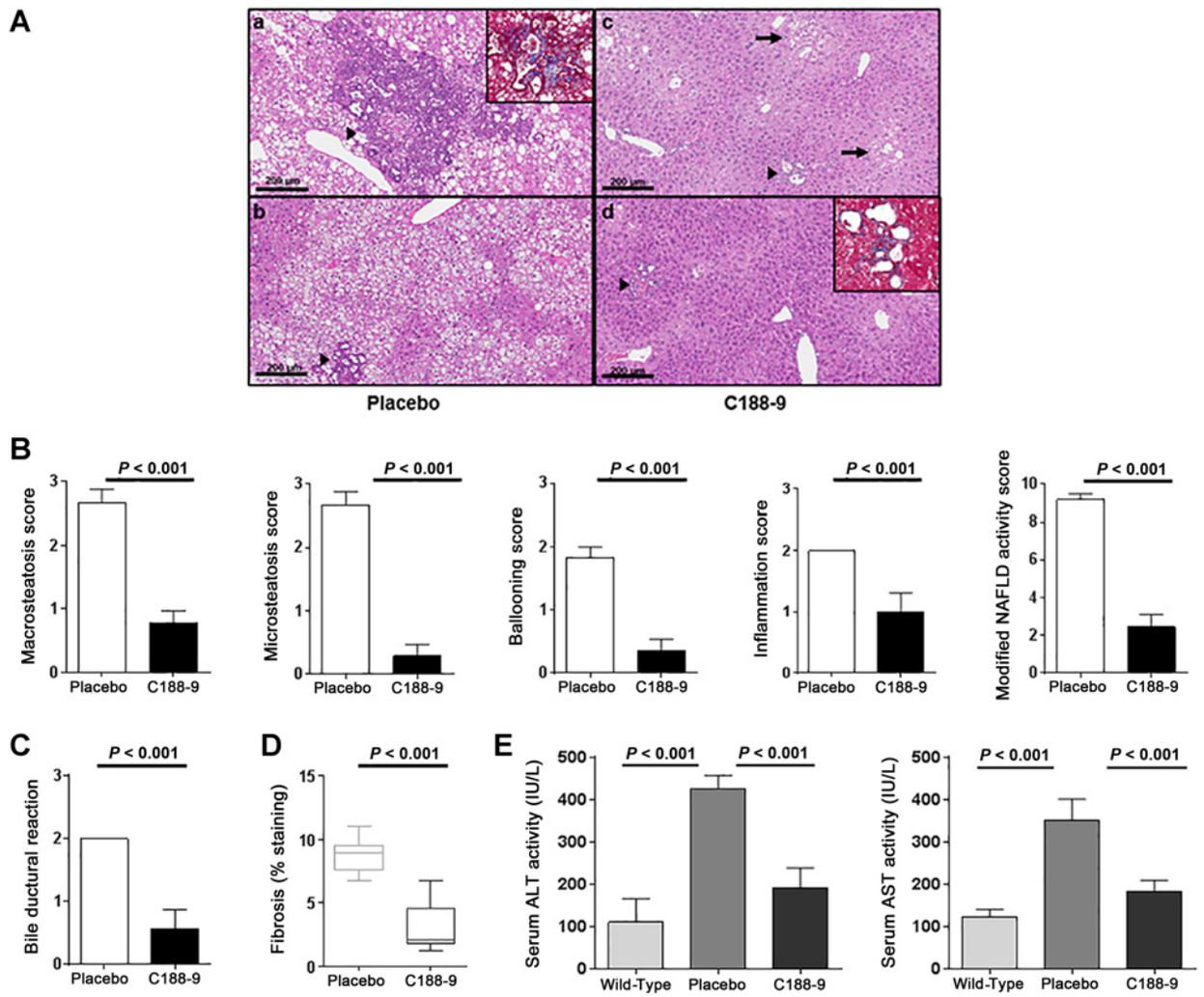

Figure 3.

Effect of C188-9 on hepatic histopathology and liver function in experimental mice. **A,** Representative images of H&E stained liver sections from vehicle- and C188-9-treated mice are shown (scale bars, 200 μm). The liver parenchyma in the vehicle-treated mice showed nearly diffuse mixed macrovesicular and microvesicular steatosis affecting all zones of hepatic lobules (from zones 1 to 3; **a** and **b**). In contrast, the livers from C188-9-treated mice showed minimal steatosis, with only a few small foci of perivenular steatosis in the centrilobular zone (**c,** arrows). The livers of vehicle-treated mice also showed frequent areas of prominent bile ductular reaction with peribiliary neutrophilic inflammation (**a** and **b,** arrow heads). Most livers of C188-9-treated mice appeared similar to untreated control mice (data not shown), with the exception of rare focal bile ductular reactions, which had less associated inflammation and were much smaller in size when compared to those observed in the vehicle group (**c** and **d,** arrowheads). Vehicle-treated mouse livers also had increased peribiliary fibrosis (**a,** inset) when compared to those from C188-9-treated mice (**d,** inset), which was confirmed by Masson's trichrome stains. **B,** Steatosis was individually scored by macrosteatosis and microsteatosis (0 for <5%, 1 for 5%–33%, 2 for 33%–66%, and 3 for more than 66%). Ballooning score was 0 for no ballooned cells per field, 1 for few, and 2 for many. Inflammation was graded by overall assessment of all inflammatory foci (0 for no foci, 1 for <2, 2 for 2–4 foci, and 3 for >4 foci). Modified NAS is the sum of marcrosteatosis, microsteatosis, inflammation, and ballooning scores. **C,** Bile ductural reaction was assessed on a 1 to 4 scale. **D,** Liver fibrosis was measured by Masson's trichrome staining. The fibrosis was quantified by determining the percentage of the positive staining area (blue staining) out of the whole liver tissue area. **E,** Serum ALT and AST levels were measured in the serum of vehicle-treated and C188-9-treated mice. For all panels, values represent mean ± SEM (Mann–Whitney test).

kinase, and interferon signaling in both liver and tumor (Supplementary Table S2). IPA analysis identified STAT3 as the main upstream regulator of the downregulated DEGs. Inhibition of STAT3 activity upon C188-9 treatment was confirmed by measuring pY-STAT3 levels, pY-STAT3 levels were increased in tumors compared to liver in the vehicle group ($P = 0.02$) confirming the activation of STAT3 in hepatocellular carcinoma in Hep*Pten*$^{-}$ mice. C188-9 treatment resulted in a reduction of pY-STAT3 levels in tumors to levels similar to those observed in vehicle-treated tumors ($P = 0.014$; Supplementary Fig. S1). TGFβ1 and IFNγ were also identified as upstream regulators in liver. In agreement, IFNγ-inducible genes and toll like receptors were overrepresented among the downregulated DEGs. A large number of profibrotic and tumor promoter genes were also found downregulated in liver and tumor (Supplementary Table S2). The effect on IFN-inducible genes suggested that STAT1 activity could also be

Published OnlineFirst May 22, 2017; DOI: 10.1158/1078-0432.CCR-16-2253

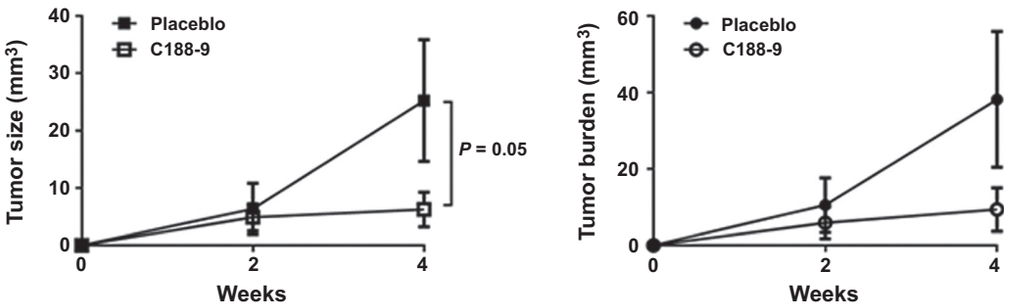

Figure 4.

Effects of C188-9 on tumor prevention *in vivo*. **A,** Average tumor volume and (**B**) average tumor burden in vehicle- and C188-9 treated Hep*Pten*$^{-}$ mice, over the 4-week treatment. Tumor volume was determined using MRI. Data are represented as mean ± SEM (Mann–Whitney test).

inhibited upon C188-9 treatment in Hep*Pten*$^{-}$ tumors. Indeed, pY-STAT1 levels were decreased upon C188-9 treatment in tumors in Hep*Pten*$^{-}$ mice ($P = 0.002$; Supplementary Fig. S1). The top biological functions and canonical pathways that were upregulated by C188-9 were FXR/RXR activation, estrogen biosynthesis and cholesterol biosynthesis in liver; granulocyte adhesion in tumor; LXR/RXR activation in both liver and tumor (Supplementary Table S3). Interestingly, Hnf4a, a major hepatocytic differentiation transcription factor, was identified as the main upstream regulator in liver, and other liver specification and differentiation genes were also upregulated such as Acox2 in liver and Hnf3a and aldolase C in tumor. A large number of cytochrome P450 genes were upregulated in both liver and tumor. Other genes associated with inhibition of fibrosis and tumor suppression in liver were also identified (Supplementary Table S3). We also randomly selected five genes from the list of DEGs, for validation by qRT-PCR. RNA sequencing data were validated by qRT-PCR for the downregulated genes CENPF, CD34, and HMMR, and the upregulated genes CD163 and CYP1A1 (Supplementary Fig. S2).

C188-9 treatment inhibits cell proliferation *in vivo* and is associated with reduction in circulating inflammatory chemokines

Gene expression analysis identified Ki67 as a gene commonly downregulated in both liver and tumor upon C188-9 treatment in Hep*Pten*$^{-}$ mice. Sections from vehicle and C188-9 treated tumor were stained with Ki67 antibody, and the percentages of Ki67-positive cells were calculated. As shown in Fig. 6A, C188-9 treated

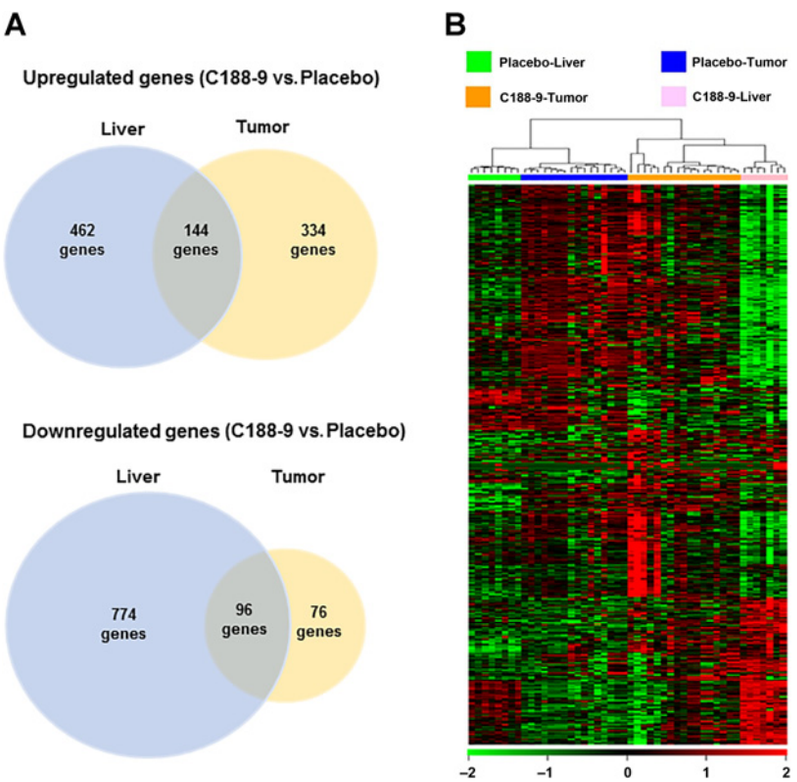

Figure 5.

Clustering of differentially expression genes. **A,** Venn diagrams showing upregulated and downregulated genes in C188-9 vs. vehicle-treated liver and in C188-9 vs. vehicle-treated tumors. The diagram shows the number of genes identified in each group following the criteria described in the Materials and Methods section. **B,** Hierarchical clustering and heat map of 1,868 differentially expressed genes in samples from four groups (vehicle livers, vehicle tumors, C188-9 livers, and C188-9 tumors). Green color indicates strength of C188-9-induced downregulation and red indicates upregulation.

Published OnlineFirst May 22, 2017; DOI: 10.1158/1078-0432.CCR-16-2253

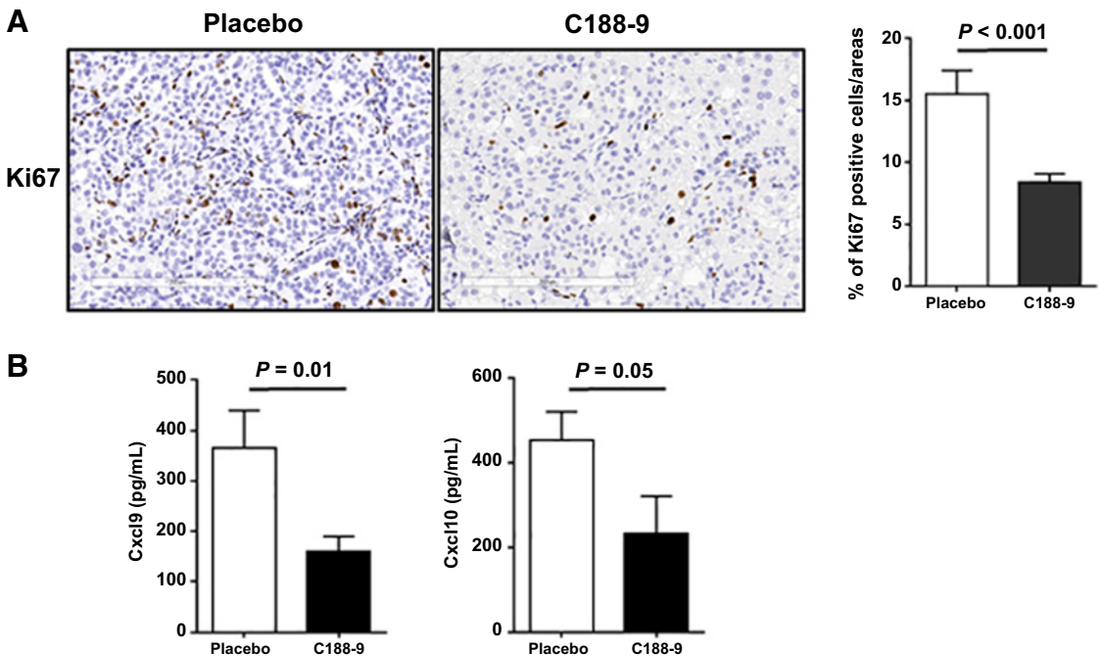

Figure 6.

Effects of C188-9 treatment on tumor cell proliferation and chemokine levels in serum. In both vehicle and C188-9-treated mice, Ki67 IHC staining was used to evaluate the amount of tumor cell proliferation. **A,** Representative sections are shown. Scale bars, 200 μm. **B,** Quantitation of IHC-positive staining for Ki67 expressed as percentage of positive tumor cells. **C,** Serum levels of CXCL9 and CXCL10 in vehicle- and C188-9-treated Hep*Pten*$^{-}$ mice. Values represent mean ± SEM (Mann–Whitney test).

group exhibited less staining for Ki67, when compared with the vehicle treated group (15.5 ± 1.9 vs. 8.4 ± 0.7; $P < 0.001$). Because inflammation was reduced based on histology analysis and because several inflammatory cytokines and chemokines were found modulated by C188-9 in gene expression analysis, we measured a panel of cytokines/chemokines in serum collected from the mice treated with either vehicle or C188-9. CXCL9 and CXCL10 levels were found to be dramatically decreased in C188-9-treated mice (364.6 ± 75.2 pg/mL vs. 159.9 ± 30.6 pg/mL, $P = 0.01$ and 455.1 ± 66.7 pg/mL vs. 234.0 ± 87.7 pg/mL, $P = 0.05$, respectively; Fig. 6B).

Discussion

Although causal roles for STAT3 in hepatic tumorigenesis have been proposed (32), the importance of STAT3 in hepatocellular carcinoma preconditions, such as liver fibrosis or NASH, has received far less attention, aside from two studies suggesting that STAT3 inhibition mediates the antifibrotic effect of sorafenib (33) and that STAT3 signaling is activated in NAFLD (34). Herein, we used a clinically relevant model of NASH-associated hepatocellular carcinoma to evaluate the therapeutic potential of C188-9, a small molecule inhibitor of STAT3. C188-9 binds to the SH2 domain of STAT3 and blocks its recruitment to the kinase-containing receptor complexes, its tyrosine phosphorylation, and its homodimerization. STAT3 activation can lead to tumorigenesis in diverse type of cancers (18–21). We demonstrated that C188-9 had beneficial effects on both hepatic tumor and NASH in liver, with blockage of tumor growth and progression, prevention of tumor development, reduction of steatosis, inflammation, and hepatocellular ballooning, resulting in NASH reversion, and reduction of bile ductular reaction and associated fibrosis. Evaluation of C188-9 treatment on additional models of hepatocellular carcinoma and NASH will be needed to demonstrate that the effects reported in this study are independent of hepatic PTEN loss. Future studies aimed at further characterizing STAT3 activation in human NASH-hepatocellular carcinomas are also warranted.

Genomic analysis identified a main inhibitory effect on immune response including downregulation of TREM-1 signaling and reduced expression of Toll-like receptors (TLR) and interferon-inducible genes. It was previously reported that the proinflammatory myeloid cell receptor TREM-1 controls development of hepatocellular carcinoma (35) and that TREM-1 expression in hepatic stellate cells is a prognostic marker for hepatitis B-related hepatocellular carcinoma (36). TLRs are pattern recognition receptors that sense and respond to microbial pathogens and damage-associated molecular patterns by facilitating inflammation (37). TLR are present on host immune cells, especially macrophages and dendritic cells, but also on epithelial cells (38). STAT3 is an important regulator of TLR2 and TLR4 activity and a mediator of TLR4 and TLR9 signaling (39–42). TLR3/4/9-mediated inflammatory responses are an important contributor of chronic inflammation-associated hepatocellular carcinoma (43). The reduction of TLRs in C188-9 treated Hep*Pten*$^{-}$ mice may contribute to the concomitant reduction in inflammation measured by histology and in reduced levels of inflammatory cytokines in serum of these mice and in the overall reduction of NASH severity. TLR2, TLR4, and TLR9 has been implicated in the development of ASH, NASH, liver fibrosis, and hepatocellular

Published OnlineFirst May 22, 2017; DOI: 10.1158/1078-0432.CCR-16-2253

carcinoma and increased TLRs is involved in increased inflammation in these chronic liver disease (44–47). Whether the observed reduction in TLRs in liver and tumor upon C188-9 treatment corresponds to a reduction in immune cell infiltration or a reduced expression on epithelial cells or both requires further evaluation. A comprehensive immune profiling follow-up study aimed at identifying the immune cell populations affected by C188-9 treatment in the Hep*Pten*$^{-}$ model would be highly relevant. Such populations include Th2 and Th17 cells: STAT3 drives development of Th17 cells and cytokine production by Th2 and Th17 cells and we have recently reported that C188-9 prevents the accumulation of Th2 and Th17 cells in a murine asthma model (48).

In contrast, the Farnesoid X receptor (FXR) signaling pathway was activated upon C188-9 treatment. FXR is highly expressed in liver and has an important role in protecting against hepatocellular carcinoma by inhibiting cell growth and inducing cell cycle arrest at G_1 phase (49). Genomic analysis also identified HNF4a, a major hepatocytic transcription factor, as the main upstream regulator in liver and other liver specification genes upregulated in liver and tumor, suggesting that C188-9 induced hepatocytic differentiation in both liver and tumor. We recently showed that induction of hepatocytic differentiation in the Hep*Pten*$^{-}$ model inhibits tumor growth, reduced liver fibrosis and prevented tumor development (7). Therefore, the improved differentiation status of hepatic cells may contribute to the therapeutic effect of C188-9 treatment on tumor and liver and the observed improvement in liver injury tests.

C188-9 has been shown to have inhibitory effects on STAT1 in prior studies involving head and neck squamous cell carcinoma (20). Although we identified STAT3 as the main upstream regulator targeted by C188-9 treatment in both liver and tumor, the significant overrepresentation of interferon-inducible genes among the C188-9-dependent downregulated genes, suggested that STAT1 activity was also inhibited. C188-9-induced inhibition of STAT1 activity was indeed confirmed in both liver and hepatic tumors. The differential contribution of inhibition of STAT1 versus STAT3 to the C188-9 treatment effects in Hep*Pten*- model will be further investigated in follow-up studies.

In conclusion, this study identified the novel small-molecule C188-9 as a highly promising therapeutic drug for treatment and prevention of hepatocellular carcinoma. C188-9 showed not only preventive and antitumor activity but also significant reduced pathologic lesions of NASH and hepatocellular injury, with an overall improvement of liver functions. This dual effect of C188-9 may be highly beneficial to patients with hepatocellular carcinoma with NASH or liver cirrhosis. A phase I trial will be initiated later this year to examine the potential of C188-9 treatment in patients with hepatocellular carcinoma.

Disclosure of Potential Conflicts of Interest

D.J. Tweardy is an employee of and holds ownership interest (including patents) in StemMed, Ltd. No potential conflicts of interest were disclosed by the other authors.

Authors' Contributions

Conception and design: D.J. Tweardy, L. Beretta
Development of methodology: D.J. Tweardy
Acquisition of data (provided animals, acquired and managed patients, provided facilities, etc.): H. Shen, M. Gagea, T.K. Eckols, L. Beretta
Analysis and interpretation of data (e.g., statistical analysis, biostatistics, computational analysis): K.H. Jung, W. Yoo, H.L. Stevenson, D. Deshpande, M. Gagea, S.-Y. Yoo, J. Wang, T.K. Eckols, U. Bharadwaj, L. Beretta
Writing, review, and/or revision of the manuscript: K.H. Jung, W. Yoo, H.L. Stevenson, D. Deshpande, M. Gagea, U. Bharadwaj, D.J. Tweardy, L. Beretta
Administrative, technical, or material support (i.e., reporting or organizing data, constructing databases): T.K. Eckols, D.J. Tweardy
Study supervision: L. Beretta

Grant Support

This work was supported in part by the NIH through Cancer Center Support grant (P30CA016672 to L. Beretta), by the Sequencing and Microarray Facility at the University of Texas MD Anderson Cancer Center CA016672, and by Cancer Prevention and Research Institute of Texas grant (DP150069 to D. Tweardy).

The costs of publication of this article were defrayed in part by the payment of page charges. This article must therefore be hereby marked *advertisement* in accordance with 18 U.S.C. Section 1734 solely to indicate this fact.

Received September 8, 2016; revised January 16, 2017; accepted May 16, 2017; published OnlineFirst May 22, 2017.

References

1. Jemal A, Bray F, Center MM, Ferlay J, Ward E, Forman D. Global cancer statistics. CA Cancer J Clin 2011;61:69–90.
2. El-Serag HB. Hepatocellular carcinoma: recent trends in the United States. Gastroenterology 2004;127(5 Suppl 1):S27–34.
3. Ryerson AB, Eheman CR, Altekruse SF, Ward JW, Jemal A, Sherman RL, et al. Annual Report to the Nation on the Status of Cancer, 1975–2012, featuring the increasing incidence of liver cancer. Cancer 2016;122:1312–37.
4. Tanaka S, Arii S. Molecular targeted therapies in hepatocellular carcinoma. Semin Oncol 2012;39:486–92.
5. Cervello M, McCubrey JA, Cusimano A, Lampiasi N, Azzolina A, Montalto G. Targeted therapy for hepatocellular carcinoma: novel agents on the horizon. Oncotarget 2012;3:236–60.
6. Muntane J, De la Rosa AJ, Docobo F, Garcia-Carbonero R, Padillo FJ. Targeting tyrosine kinase receptors in hepatocellular carcinoma. Curr Cancer Drug Targets 2013;13:300–12.
7. Bruix J, Sherman M, American Association for the Study of Liver D. Management of hepatocellular carcinoma: an update. Hepatology 2011;53:1020–2.
8. Kim H, Park YN. Hepatocellular carcinomas expressing 'stemness'-related markers: clinicopathological characteristics. Dig Dis 2014;32:778–85.
9. Jing N, Tweardy DJ. Targeting Stat3 in cancer therapy. Anticancer Drugs 2005;16:601–7.
10. Furtek SL, Backos DS, Matheson CJ, Reigan P. Strategies and approaches of targeting STAT3 for cancer treatment. ACS Chem Biol 2016;11:308–18.
11. Bharadwaj U, Kasembeli MM, Tweardy DJ. STAT3 inhibitors in cancer: a comprehensive update. In: Ward AC, editor. STAT inhibitors in cancer. Switzerland: Springer International Publishing; 2016.
12. Calvisi DF, Ladu S, Gorden A, Farina M, Conner EA, Lee JS, et al. Ubiquitous activation of Ras and Jak/Stat pathways in human HCC. Gastroenterology 2006;130:1117–28.
13. He G, Yu GY, Temkin V, Ogata H, Kuntzen C, Sakurai T, et al. Hepatocyte IKKbeta/NF-kappaB inhibits tumor promotion and progression by preventing oxidative stress-driven STAT3 activation. Cancer Cell 2010;17:286–97.
14. Won C, Kim BH, Yi EH, Choi KJ, Kim EK, Jeong JM, et al. Signal transducer and activator of transcription 3-mediated CD133 up-regulation contributes to promotion of hepatocellular carcinoma. Hepatology 2015;62:1160–73.
15. He G, Karin M. NF-kappaB and STAT3 - key players in liver inflammation and cancer. Cell Res 2011;21:159–68.

16. Wang H, Lafdil F, Kong X, Gao B. Signal transducer and activator of transcription 3 in liver diseases: a novel therapeutic target. Int J Biol Sci 2011;7:536–50.
17. Wang B, Hsu SH, Frankel W, Ghoshal K, Jacob ST. Stat3-mediated activation of microRNA-23a suppresses gluconeogenesis in hepatocellular carcinoma by down-regulating glucose-6-phosphatase and peroxisome proliferator-activated receptor gamma, coactivator 1 alpha. Hepatology 2012;56:186–97.
18. Xu X, Kasembeli MM, Jiang X, Tweardy BJ, Tweardy DJ. Chemical probes that competitively and selectively inhibit Stat3 activation. PLoS One 2009;4:e4783.
19. Redell MS, Ruiz MJ, Alonzo TA, Gerbing RB, Tweardy DJ. Stat3 signaling in acute myeloid leukemia: ligand-dependent and -independent activation and induction of apoptosis by a novel small-molecule Stat3 inhibitor. Blood 2011;117:5701–9.
20. Bharadwaj U, Eckols TK, Xu X, Kasembeli MM, Chen Y, Adachi M, et al. Small-molecule inhibition of STAT3 in radioresistant head and neck squamous cell carcinoma. Oncotarget 2016;7:26307–30.
21. Lewis KM, Bharadwaj U, Eckols TK, Kolosov M, Kasembeli MM, Fridley C, et al. Small-molecule targeting of signal transducer and activator of transcription (STAT) 3 to treat non-small cell lung cancer. Lung Cancer 2015;90:182–90.
22. Horie Y, Suzuki A, Kataoka E, Sasaki T, Hamada K, Sasaki J, et al. Hepatocyte-specific Pten deficiency results in steatohepatitis and hepatocellular carcinomas. J Clin Invest 2004;113:1774–83.
23. Stiles B, Wang Y, Stahl A, Bassilian S, Lee WP, Kim YJ, et al. Liver-specific deletion of negative regulator Pten results in fatty liver and insulin hypersensitivity [corrected]. Proc Natl Acad Sci U S A 2004;101:2082–7.
24. Lai KK, Shang S, Lohia N, Booth GC, Masse DJ, Fausto N, et al. Extracellular matrix dynamics in hepatocarcinogenesis: a comparative proteomics study of PDGFC transgenic and Pten null mouse models. PLoS Genet 2011;7:e1002147.
25. Muir K, Hazim A, He Y, Peyressatre M, Kim DY, Song X, et al. Proteomic and lipidomic signatures of lipid metabolism in NASH-associated hepatocellular carcinoma. Cancer Res 2013;73:4722–31.
26. Zhang J, Jiao J, Cermelli S, Muir K, Jung KH, Zou R, et al. miR-21 inhibition reduces liver fibrosis and prevents tumor development by inducing apoptosis of CD24+ progenitor cells. Cancer Res 2015;75:1859–67.
27. Jung KH, Zhang J, Zhou C, Shen H, Gagea M, Rodriguez-Aguayo C, et al. Differentiation therapy for hepatocellular carcinoma: Multifaceted effects of miR-148a on tumor growth and phenotype and liver fibrosis. Hepatology 2016;63:864–79.
28. Kleiner DE, Brunt EM, Van Natta M, Behling C, Contos MJ, Cummings OW, et al. Design and validation of a histological scoring system for nonalcoholic fatty liver disease. Nonalcoholic Steatohepatitis Clinical Research Network. Hepatology 2005;41:1313–21.
29. Trapnell C, Pachter L, Salzberg SL. TopHat: discovering splice junctions with RNA-Seq. Bioinformatics (Oxford, England) 2009;25:1105–11.
30. Aktas B, Tewes M, Fehm T, Hauch S, Kimmig R, Kasimir-Bauer S. Stem cell and epithelial-mesenchymal transition markers are frequently overexpressed in circulating tumor cells of metastatic breast cancer patients. Breast Cancer Res 2009;11:R46.
31. Kim BK, Lee JW, Park PJ, Shin YS, Lee WY, Lee KA, et al. The multiplex bead array approach to identifying serum biomarkers associated with breast cancer. Breast Cancer Res 2009;11:R22.
32. Wong AL, Soo RA, Tan DS, Lee SC, Lim JS, Marban PC, et al. Phase I and biomarker study of OPB-51602, a novel signal transducer and activator of transcription (STAT) 3 inhibitor, in patients with refractory solid malignancies. Ann Oncol 2015;26:998–1005.
33. Su TH, Shiau CW, Jao P, Liu CH, Liu CJ, Tai WT, et al. Sorafenib and its derivative SC-1 exhibit antifibrotic effects through signal transducer and activator of transcription 3 inhibition. Proc Natl Acad Sci U S A 2015;112:7243–8.
34. Min H-K, Mirshahi F, Verdianelli A, Pacana T, Patel V, Park C-G, et al. Activation of the GP130-STAT3 axis and its potential implications in nonalcoholic fatty liver disease. Am J Physiol Gastrointest Liver Physiol 2015;308:G794–803.
35. Wu J, Li J, Salcedo R, Mivechi NF, Trinchieri G, Horuzsko A. The proinflammatory myeloid cell receptor TREM-1 controls Kupffer cell activation and development of hepatocellular carcinoma. Cancer Res 2012;72:3977–86.
36. Liao R, Sun TW, Yi Y, Wu H, Li YW, Wang JX, et al. Expression of TREM-1 in hepatic stellate cells and prognostic value in hepatitis B-related hepatocellular carcinoma. Cancer Sci 2012;103:984–92.
37. Kawai T, Akira S. Toll-like receptors and their crosstalk with other innate receptors in infection and immunity. Immunity 2011;34:637–50.
38. Shaykhiev R, Behr J, Bals R. Microbial patterns signaling via Toll-like receptors 2 and 5 contribute to epithelial repair, growth and survival. PLoS One 2008;3:e1393.
39. Tye H, Kennedy CL, Najdovska M, McLeod L, McCormack W, Hughes N, et al. STAT3-driven upregulation of TLR2 promotes gastric tumorigenesis independent of tumor inflammation. Cancer Cell 2012;22:466–78.
40. Greenhill CJ, Rose-John S, Lissilaa R, Ferlin W, Ernst M, Hertzog PJ, et al. IL-6 trans-signaling modulates TLR4-dependent inflammatory responses via STAT3. J Immunol 2011;186:1199–208.
41. Yu H, Lee H, Herrmann A, Buettner R, Jove R. Revisiting STAT3 signalling in cancer: new and unexpected biological functions. Nat Rev Cancer 2014;14:736–46.
42. Eyking A, Ey B, Runzi M, Roig AI, Reis H, Schmid KW, et al. Toll-like receptor 4 variant D299G induces features of neoplastic progression in Caco-2 intestinal cells and is associated with advanced human colon cancer. Gastroenterology 2011;141:2154–65.
43. Li W, Xiao J, Zhou X, Xu M, Hu C, Xu X, et al. STK4 regulates TLR pathways and protects against chronic inflammation-related hepatocellular carcinoma. J Clin Invest 2015;125:4239–54.
44. Roh YS, Seki E. Toll-like receptors in alcoholic liver disease, non-alcoholic steatohepatitis and carcinogenesis. J Gastroenterol Hepatol 2013;28Suppl 1:38–42.
45. Sawada K, Ohtake T, Hasebe T, Abe M, Tanaka H, Ikuta K, et al. Augmented hepatic Toll-like receptors by fatty acids trigger the pro-inflammatory state of non-alcoholic fatty liver disease in mice. Hepatol Res 2014;44:920–34.
46. Miura K, Ohnishi H. Role of gut microbiota and Toll-like receptors in nonalcoholic fatty liver disease. World J Gastroenterol 2014;20:7381–91.
47. Kapil S, Duseja A, Sharma BK, Singla B, Chakraborti A, Das A, et al. Small intestinal bacterial overgrowth and toll-like receptor signaling in patients with non-alcoholic fatty liver disease. J Gastroenterol Hepatol 2016;31:213–21.
48. Gavino AC, Nahmod K, Bharadwaj U, Makedonas G, Tweardy DJ. STAT3 inhibition prevents lung inflammation, remodeling, and accumulation of Th2 and Th17 cells in a murine asthma model. Allergy 201671:1684–92.
49. Guo F, Xu Z, Zhang Y, Jiang P, Huang G, Chen S, et al. FXR induces SOCS3 and suppresses hepatocellular carcinoma. Oncotarget 2015;6:34606–16.

Published OnlineFirst May 22, 2017; DOI: 10.1158/1078-0432.CCR-16-2253

Clinical Cancer Research

Multifunctional Effects of a Small-Molecule STAT3 Inhibitor on NASH and Hepatocellular Carcinoma in Mice

Kwang Hwa Jung, Wonbeak Yoo, Heather L. Stevenson, et al.

Clin Cancer Res 2017;23:5537-5546. Published OnlineFirst May 22, 2017.